In Vitro Reconstitution of Recognition and Activation Complexes between Interleukin-6 and gp130†

Dar-chone Chow,‡ Joseph Ho,‡ Thuy Linh Nguyen Pham,‡ Stefan Rose-John,§ and K. Christopher Garcia*,‡

Departments of Microbiology & Immunology, and Structural Biology, Stanford University School of Medicine, Fairchild D319, 299 Campus Drive, Stanford, California 94305-5124, and Department of Biochemistry, Christian-Albrechts-Universität zu Kiel, Olshausenstrasse 40, D-24098 Kiel, Germany

Received January 30, 2001; Revised Manuscript Received April 18, 2001

ABSTRACT: Gp130 is a shared signal-transducing receptor for a family of four-helix cytokines, of which interleukin-6 is a prototypic member. IL-6-type cytokines activate gp130 to elicit downstream intracellular JAK/STAT signaling cascades through formation of hetero-oligomeric receptor complexes. Interleukin-6 must first complex with its specific α-receptor (Rα) in order to bind and activate gp130. We have dissected the extracellular activation pathway of human gp130 by human IL-6 through reconstitution of soluble complexes representing intermediate and final states in the hierarchical assembly of the IL-6/IL-6Rα/gp130 signaling complex. To isolate these hetero-complexes, we have applied a protein engineering strategy of covalently linking IL-6 to its Rα, which results in a "hyperactive" single-chain complex (hyper-IL-6) which we express in both *Escherichia coli* and insect cells. We have determined that IL-6/IL-Rα and the cytokine-binding homology region (CHR) of gp130 (D2D3) form a stable trimolecular "recognition" complex (trimer) consisting of 1IL-6,1 IL-6Rα, and 1 gp130-CHR. Addition of the N-terminal (D1) Ig-like domain (IGD) of gp130 to the CHR results in a transition to a hexameric "activation" complex containing 2 IL-6, 2IL-6Rα, and 2 gp130. These results clearly demonstrate that the recognition and activation complexes are disparate hetero-oligomeric molecular species linked by the recruitment of the gp130 IGD by the unique site III epitope present on all gp130-class cytokines. The results of these studies are relevant to other members of the IL-6 family of gp130-cytokines and address a longstanding question concerning the respective roles of the gp130 CHR and IGD in assembly of the active signaling oligomer.

The ligand-mediated clustering of receptor extracellular domains into unique macromolecular orientations, which elicit defined intracellular signaling cascades, has emerged as a central paradigm in biology as a means for a cell to respond to its environment. Cytokines are particularly important intercellular mediators of a diverse spectrum of physiological functions, including growth regulation, hematopoiesis, angiogenesis, neuronal growth, host defense, and pro-inflammatory responses. Cytokines carry out their functions by engaging relatively conserved structural motifs on cell-surface receptors, which results in phosphorylation of intracellular signal transduction molecules (*1*).

Gp130 is a cytokine receptor which is a shared signal transducer for a family of four-helix bundle cytokines including interleukin-6 (IL-6),[1] viral IL-6, leukemia inhibitory factor (LIF), ciliary neurotrophic factor (CNTF), oncostatin M (OSM), interleukin-11 (IL-11), and cardiotrophin 1 (CT1) (*2*−*5*). Gp130 signaling is critical to the normal growth and differentiation of numerous tissue types and derangements in gp130 signaling have been implicated in a large number of diseases and neoplastic disorders, such as multiple myeloma. gp130-cytokines carry out their functions though formation of hetero-oligomeric receptor complexes containing the gp130 signal transducing receptor, which leads to intracellular activation of src and JAK/Tyk tyrosine kinases, as well as the STAT family of transcription factors (*2*). Interleukin-6 was the first cytokine discovered to signal through gp130, and is the best studied of the family of gp130-cytokines, also referred to as "IL-6-type" cytokines (*6*, *7*). Interleukin-6 (IL-6) is a pro-inflammatory cytokine and plays a central role in host defense against infection and tissue injuries (*7*). The activities of IL-6 are highly pleiotropic, stimulating a wide range of biological activities including B cell maturation, hepatocyte regeneration, and neuronal growth (*3*).

† D.-c.C is supported by a postdoctoral training grant to the Department of Microbiology & Immunology, and K.C.G. is supported by the Cancer Research Institute, the California Cancer Research Program, a Rita Allen Foundation award, a Frederick Terman Junior Faculty award, NIH (RO1-AI-48540-01), and startup funds provided by The Stanford University School of Medicine.

* To whom correspondence should be addressed. E-mail: kcgarcia@stanford.edu. Phone: (650) 498-7332. Fax: (650) 725-6757.

‡ Departments of Microbiology & Immunology, and Structural Biology.

§ Department of Biochemistry.

[1] Abbreviations: Rα, IL-6 α-receptor; IL-6, interleukin-6; IL-6/IL-6Rα, the complex of IL-6 and the IL-6 Rα; hyper-IL-6, single-chain IL-6/IL-6Rα; CHR, cytokine-binding homology region; IGD, immunoglobulin-like domain; D2D3, domains 2 and 3; D1D2D3, domains 1, 2, and 3; gp130-CHR, the cytokine-binding homology region (CHR) of gp130 (D2D3); gp130-IGD-CHR, the immunoglobulin-like domain of gp130 (D1) plus the CHR (D2D3); recognition complex, IL-6/IL-6Rα/gp130-CHR; activation complex, IL-6/IL-6Rα/gp130-IGD-CHR; AU, analytical ultracentrifugation; BIAcore, surface plasmon resonance; RU, resonance units; GFC, gel filtration chromatography; kDa, kilodaltons; Mr, relative mass.

10.1021/bi010192q CCC: $20.00
Published on Web 06/02/2001

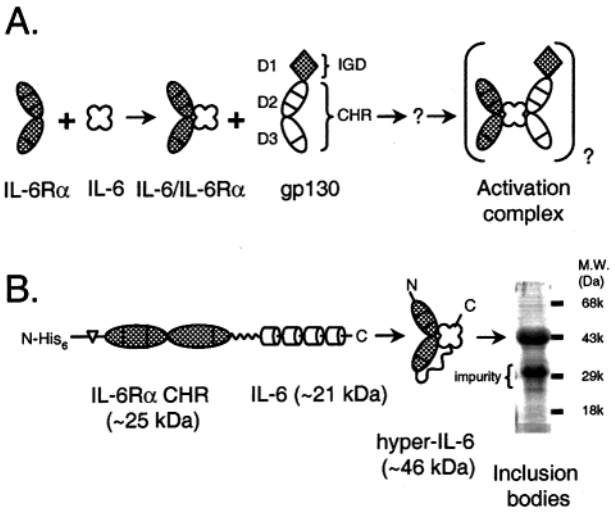

FIGURE 1: Assembly of the IL-6, IL-6 α-receptor, and gp130 complexes. (A) IL-6 first complexes with IL-6Rα which in turn complexes with gp130. The IL-6/IL-6Rα/gp130 trimer further matures into a higher order complex involving at least two gp130s. The order of the interactions and the stoichiometry of the complexes are unclear as marked by "?". (B) Design and expression of "hyper-IL-6". IL-6 is linked to the C-terminus of the IL-6Rα (D2D3) CHR domain via a 15-amino acid Gly-Ser linker, and a Hexa-Histidine tag is appended to the N-terminus of IL-6Rα CHR via a thrombin-cleavable linker. At the far right is shown a coommassie-stained SDS−PAGE of the inclusion bodies of the single chain fusion protein. The inclusion bodies are approximately 75% pure, with only one major contaminant.

IL-6-type cytokines share a common, classical four-helix bundle fold originally described by Bazan (*7*−*9*). The receptor-binding properties of IL-6, and other gp130-cytokines, have been extensively analyzed through structure−function studies which have revealed that gp130 engagement occurs through three conserved receptor-binding epitopes on the cytokines, the third of which is unique to gp130-cytokines (*5*, *7*). The first epitope, termed site I, binds to a nonsignaling α-receptor, and the second and third epitopes, sites II and III, are specific for gp130 (Figure 1A). The extracellular region of gp130 is composed of six modular β-sheet sandwich domains. Cytokine engagement by the gp130 extracellular region occurs through three membrane-distal, β-sheet sandwich domains (D1D2D3) (Figure 1A) (*10*). The three membrane-proximal fibronectin type-III domains do not play a specific role in recognition, but have been implicated in receptor−receptor contact in the gp130 homodimer (*11*). The cytokine-binding homology region (CHR) (Figure 1A) of gp130 is located at domains 2 and 3 (D2D3) and contains the signature WSXWS box and characteristic pattern of cysteines which are hallmark patterns of CHR's on all cytokine receptors (*8*). However, gp130 uniquely requires an additional N-terminal (D1) Ig-like activation domain (IGD) in order to be functionally responsive to cytokine (*12*). The structure, role, and disposition of this IGD in recognition and activation is not known.

The molecular basis by which IL-6 activates gp130 is distinct from other members of the hematopoietic receptor family typified by the simpler, but paradigmatic, human growth hormone (hGH) and erythropoeitin (EPO) systems (*13*, *14*). Interleukin-6 must first complex with a specific, nonsignaling α receptor (termed IL-6Rα), though a "site I" epitope, to acquire the ability to bind gp130 (Figure 1A) (*4*). This binary complex of IL-6 and Rα, then forms a composite epitope, termed "site II," which is capable of activating gp130 (Figure 1A) (*7*, *9*). A transition to a higher-order signaling assembly is a second defining feature of IL-6-type cytokines (Figure 1A) and is mediated through a functional interaction between the unique third receptor-binding epitope (site III) and the gp130 activation domain (D1 or IGD) (*12*, *15*−*17*): it has not been known whether there is a direct structural interaction. A number of functional studies indicate that IL-6-type signaling complexes are "hexamers" containing two copies of cytokine, Rα, and gp130 (2:2:2) (*18*−*20*). Hence, unlike the classical models of cytokine receptor homodimerization by hGH, IL-6 requires heterodimerization as well as oligomerization. These characteristics significantly increase the complexity of the system and present obstacles to deconvoluting the individual receptor−ligand interactions within the larger assembly.

In the present study, we examine a number of longstanding questions concerning the mechanism of assembly of the higher-order IL-6/gp130 signaling complex using engineered, soluble recombinant proteins. In particular, we address the issues of (1) the stoichiometries of the hetero-oligomeric IL-6/IL-6Rα/gp130 complexes, (2) whether the assembly of the higher-order signaling complex is preceded by a lower-order complex, and (3) whether the ability of the CHR to engage cytokine is dependent on the presence of the structurally distinct N-terminal IGD of gp130 in receptor activation. Since our aim is to study the interaction between the prerequisite IL-6/IL-6Rα complex with gp130, we utilize a functional single-chain IL-6/IL-6Rα complex (*21*) to simplify the interaction from a three body problem (IL-6/IL-6Rα/gp130) into a discrete bimolecular two-body problem (single-chain IL-6-IL-6Rα/gp130) (Figure 1). Using this strategy we have produced stable, soluble complexes of single-chain IL-6/IL-6Rα [also called "hyper-IL-6"(*21*)] with both the gp130 CHR (D2D3) and the full activation fragment gp130 IGD-CHR (D1D2D3). We find that the hyper-IL-6 binds with moderate affinity to the gp130 CHR, and forms a trimolecular (1:1:1) complex. We also determine that hyper-IL-6 complexed to the gp130 IGD-CHR (D1D2D3) forms a hexameric complex (2:2:2) of greater stability. Hence, the activation pathway of gp130 can be dissected into separable "recognition" and "activation" complexes which are sequential and cooperative. We propose that the single-chain technology can be utilized as a general tool for investigation of macromolecular complex formation involving multiple bimolecular interactions.

MATERIALS AND METHODS

Materials. AKTA FPLC system, Superdex 200 HR10/30 column, and the PhastSystem were from Amersham Pharmacia Biotech AB (Uppsala, Sweden), and Ni-NTA agarose were from QIAGEN (Hilden, Germany). Pfu DNA polymerase was from Promega. pET DNA vectors were from Novagen (Madison, WI). IPTG was purchased from Applied Scientific, and all other chemicals from Fisher Scientific or Sigma Chemical Co. Restriction enzymes were from New England Biolabs.

Gp130 CHR Domain Expression Vector. The DNA fragment corresponding to gp130 cytokine-binding homology region (CHR, amino acids 121−291) was generated using

PCR with primers: forward 5′ATG CAA GAA TTC TCA GGC TTG CCT CCA GAA AAAA CCT AAA (underline is the *Eco*RI site) and backward 5′ATG CAA AAG CTT TCA GTG ATG GTG ATG GTG ATG TGG TCT ATC TTC ATA GGT GAT CCC (underline is the *Hin*dIII site, followed by a stop codon and a 6-His tag), using human gp130 cDNA. The PCR product was digested with *Eco*RI and *Hin*dIII, gel purified with QIAEX II gel extraction kit (QIAGEN), and then subcloned in pET 24a vector on *Eco*RI and *Hin*dIII sites. The C-terminus of the expressed peptide fragment contains a 6× His tag.

Gp130 IGD-CHR Expressing Recombinant Baculovirus. The DNA fragment corresponding to the gp130 IGD and CHR domains (amino acids 1−291) was generated using PCR with forward primer 5′ATG CAA GGA TCC CGA ACT TCT AGA TCC ATG TGG TTA TAT C (underline is the *Bam*HI site) and backward primer 5′ATG CAA GAA TTC TCA GTG ATG GTG ATG GTG ATG TGG TCT ATC TTC ATA GGT GAT CCC (underline is the *Eco*RI site, followed by a stop codon and a 6× His tag) using human gp130 DNA.This PCR product was digested with *Bam*HI and *Eco*RI and subcloned into the transfer vector pAcGP67A (PharMingen). To produce the recombinant Baculovirus, *Spodoptera frugiperda* (**Sf9**) cells were transfected with a combination of the recombinant transfer vectors and a linearized AcNPV DNA (BaculoGold) using CELLFectin (Invitrogen) according to the protocol provided by PharMingen (San Diego, CA). Baculovirus containing recombinant DNA was amplified in Sf9 cells in a serum-containing medium.

Hyper-IL-6 Expression Vector. The hyper-IL-6 cDNA was previously reported (*21*) and cloned into pET28a vector via sites *Nde*I and *Hin*dIII at the 5′ and 3′ ends, respectively. The expressed hyper-IL-6 contains a thrombin cleavable N-terminal 6-His tag.

Hyper-IL-6 Expression in Baculovirus. The transfer vector containing hyper-IL-6 was constructed similarly with forward primer 5′ATG CAA GGA TCC CCT CCT GGT AGA ATT CCC CCC C (underline is the *Bam*HI site) and backward primer5′ATG CAA TCT AGA TCA GTG ATG GTG ATG GTG ATG CAT TTG CCG AAG AGC CCT CAG (underline is the *Xha*I site). The PCR product was digested with *Bam*HI and *Xha*I and was subcloned into the transfer vector pAcGP67A. The recombinant baculovirus was produced as above. All the vectors containing PCR products DNA were sequenced to verified that no mutations had been introduced by PCR.

Refolding of the Recombinant Proteins from Inclusion Bodies. The bacteria harboring the DNA vector were grown overnight at 37 °C, then diluted 1:100 into fresh media. After reaching log phase growth ($OD_{600nm} = 0.5-0.7$), the bacteria were induced by 1 mM IPTG for 2.5 h. The bacteria were lysed by French press, the inclusion bodies were harvested by centrifugation and wash three times in TE (10 mM Tris, pH 8.0, 1 mM EDTA). The inclusion bodies was stored at 4 °C until use. A total of 70−100 mg of inclusion body was first solubilized in 6 M guanidineHCl, 50 mM Tris, pH 8, 20 mM 2ME at 37−42 °C; the solubilized proteins were diluted dropwise into 200 mL of 2 M guanidine HCl, 50 mM Tris, pH 8.0, 1 mM reduced glutathione, 0.1 mM oxidized glutathione at 4 °C. After 3 h incubation, the mixtures were diluted 5−6-fold with 200 mM NaCl, 50 mM Tris, pH 8.0, dropwise with a peristaltic pump over a period of 24−36 h. After the aggregates were filtered out with glass fiber prefilters, Ni-NTA agarose was added and incubated for 24−72 h. The Ni agaroses were harvested and the refolded proteins were eluted with 0.15−0.2 M imidazole in HBS (10 mM Hepes, pH 7.2, 150 mM NaCl). The eluted proteins were further subject to gel filtration purification on an AKTA FPLC equipped with a superdex 200 column.

Insect-Produced Recombinant Proteins. Hi5 insect cells were maintained in Insect-Express media (Biowhittaker, Walkersville, MD) with cell density $(1-5) \times 10^6$/mL. Typical infection with Baculovirus was carried out at a cell density of 1.5×10^6/mL for 3 days. Baculovirus was titrated to optimal amount in small scale (2 mL) assay prior to the large scale (1−6 L) production. The media containing the expressed recombinant proteins were centrifuged to pellet out the cell debris, 0.45 μm filtered, and then incubated with Ni-NTA agarose. After extensive washing, the Ni-NTA was eluted in 150 mM Imidazole. The eluant was further purified in either gel filtration chromatography or Mono Q ion exchange chromatography.

Surface Plasmon Resonance (SPR) Measurement of gp130 CHR Interactions with hyper-IL-6 (see Results for further discussion of methodological issues). The refolded gp130 CHR was covalently immobilized to a CM5 sensor chips via primary amino groups, using the amine coupling kit (Pharmacia Biosensor AB). Briefly, carboxylate groups on the dextran were activated by injection of a mixture of *N*-hydroxysuccinimide and *N*-ethyl-*N*′-(dimethylaminopropyl)carbodiimide. The gp130 CHR diluted with 10 mM sodium acetate, pH 5.5, was injected through the activated surface. Ethanolamine hydrochloride, pH 8.0, was injected after the immobilization to block unreacted *N*-hydroxysuccinimide esters. Running buffer in BIAcore used for washing and the dissociation phase was HBS, pH 7.4, and was identical to the buffer that used in superdex-200 chromatography. Injection buffer contains 100 μg/mL of BSA to minimize background (see Results). The hyper-IL-6 was purified by Superdex-200 chromatography prior to the BIAcore experiment. After each cycle of hyper-IL-6 association and dissociation, two blank injection cycles were run to regenerate the gp130 CHR. We also attempted to immobilize hyper-IL-6 on a CM5 sensor chip, but the immobilized hyper-IL-6 failed to bind to gp130 CHR. As a result, we are not able to perform the BIAcore analysis in a reverse orientation. For the gp130-CHR, approximately half of the immobilized gp130 CHR is not available for binding due to the random amine coupling on the BIAcore chip. Corrections were made for blank surface binding. The data were analyzed using BIAevaluation 3.0 program.

Native Gel Analysis. Native gel analysis of proteins were carried out at pH 8.0 using 10−15% PAGE gels and native gel buffer strips on the PhastSystem (Pharmacia, NJ) according to the manufacturer's protocol. The complexes were preincubated for 15 min at RT prior to electrophoresis.

Analytical Ultracentrifugation Analysis. Equilibrium sedimentation analysis was carried out in a Beckman Optima XL-A analytical ultracentrifuge equipped with an An-50 Ti titanium four-hole rotor with the 6-hole centerpieces. All the samples were centrifuged at 15 °C in HEPES-buffered saline (HBS) that contains 10 mM HEPES, pH 7.2, 150 mM NaCl. The buffer was chosen to be near the conditions of other

studies. The samples of refolded hyper-IL-6, refolded gp130 CHR, and equal molar mixture of refolded hyper-IL-6 and refolded gp130 CHR were loaded in the same cell and centrifuged at speeds of 8000, 12 000, 17 000, 20 000, 30 000 rpm, at 15 °C and then at 20 °C. The protein distribution profiles were detected with absorbance at 223, 230, and 280 nm. The mixed complex was formed an hour before loading into the cell. Hyper-IL-6/gp130 complex was loaded at three different concentrations with initial OD at 280 nm of 0.37, 0.56, 1.5, respectively (corresponding to 4, 6, and 14 μM of complex). The samples were centrifuged to equilibrium at speed of 7000, 9000, 11 000, 13 000, 15 000, 17 000, 20 000, and 25 000 rpm. The samples were centrifuged at specified speed for 20 h and distribution scans were taken. After 3 h, distribution scans were again to ensure the equilibrium has been reached. Equilibrium distributions were analyzed using winnonlin 1.06, the window version of NONLIN program. The profiles can be fitted with ideal curves with single molecular weight species according to the following equation:

$$c(r) = c(r_0)\, e^{\sigma(r^2 - r_0^2)/2}$$

where the $c(r)$ is the protein concentration at radius r and σ is the reduced molecular weight related to the molecular mass of the protein as,

$$M = \frac{\sigma \cdot R \cdot T}{(1 - \bar{\nu} \cdot \rho) \cdot \omega^2}$$

where R is the gas constant, T temperature in kelvin, $\bar{\nu}$ the protein specific volume, and ρ the buffer density. The theoretical masses and partial specific volume were calculated by AA_COMP on a MAC G3 machine. Both the protein specific volumes $\bar{\nu}$ and buffer density ρ (1.005 g/cm^3) were calculated according to Laue et al. (*22*). The partial specific volume for gp130 CHR calculated to be 0.716 cm^3/g, theoretical mass of 24.5 kDa; hyper-IL-6 has a partial specific volume of 0.732 cm^3/g, theoretical mass of 46.8 kDa; the hyper-IL-6/gp130 CHR complex has a partial specific volume of 0.731 cm^3/g and a theoretical mass of 71.3 kDa. The hyper-IL-6 has four potential N-linked glycosylation sites, and gp130 IGD-CHR has six potential N-linked glycosylation sites. Assuming they are all occupied with $(GlcNAc)_2(Man)_5$ carbohydrate moiety (each with mass of 1.34 kDa), the glycosylated dimer complex of hyper-IL-6 and gp130 IGD-CHR has a theoretical mass of 95.8 kDa, a partial specific volume of 0.72 cm^3/g, and the tetramer (hyper-IL-6/ gp130 IGD-CHR)$_2$ has a theoretical mass of 191.6 kDa.

The velocity sedimentation analysis was carried out with two-channel 12 mm path-length centerpieces. Sedimentation velocity optical absorbance scans were taken at a continuous interval mode. The sample of hyper-IL-6/gp130 CHR complex was centrifuged at 45 000 rpm at 15 and 25 °C. The sample of hyper-IL-6/gp130 IGD-CHR was centrifuged at 35 000 rpm at 20 °C. Apparent sedimentation coefficient distributions were computed by the time derivative method using dc/dt (*23*).

Biological Activity Assay of hyper-IL-6. BAF/gp130 cells have been previously described (*24*) and are maintained in a media containing 10% FBS and 50 ng/mL hyper-IL-6 and IL-3. The BAF/gp130 cells are dependent on IL-6 for growth and were plated in 96 well plates at about 10 000 cells/well. One day later, the cells were washed twice with serum free media, and replaced with serum free media containing specified amount of hyper-IL-6. Three days later, cell contents of the wells were determined using malocyte green to indicate a measure of cell proliferation.

Gel Filtration Chromatography. Gel filtration chromatography (GFC) purification and analysis were carried out at room temperature using an AKTA-FPLC system (Amersham Pharmacia Biotech). One-half of a milliliter of protein samples in buffer HBS (hepes-buffered saline, pH 7.2) was loaded on a Superdex 200 HR10/30 column (Amersham Pharmacia Biotech) preequilibrated in HBS. Fractions (0.5 mL) were collected at a flow rate of 0.5 mL/min, and the elution was monitored with optical absorbance at 280 nm. Fractions were then analyzed by SDS−PAGE. The column was calibrated with calibration standards of molecular weights ranging from 12 400 to 443 000: apo ferritin (MW = 443 000), β amylase (MW = 200 000), albumin (MW = 67 000), carbonic anhydrase (MW = 29 000), cytochrome c (MW = 12 400).

Electrophoresis. SDS−polyacrylamide gel electrophoresis (SDS−PAGE) of proteins was carried out in 0.75 or 1.5 mm thick 12% acrylamide slab gels in the Mini-Protean II apparatus from Bio-Rad according to the method of Laemmli. Protein concentrations were determined using BCA assay (Pierce, Rockford, IL).

RESULTS

Production of Recombinant Proteins. IL-6 sequentially interacts with its specific receptor α-chain (Rα) to form a binary complex that, in turn, engages the common signaling receptor, gp130, to initiate a JAK/STAT intracellular activation cascade. To create a high-potency version of IL-6 for potential clinical applications, Fischer et al. (*21*) designed a fusion protein linking IL-6 to the cytokine-binding homology region (CHR, domains 2 and 3) of IL-6Rα. This fusion protein, called hyper-IL-6, is a highly potent stimulator of gp130 due to the elimination of dissociation of IL-6 and IL-6Rα. We have utilized this approach in this study to simplify in vitro measurements of the interactions of the IL-6/IL-6Rα complex with gp130, simplifying a three-body problem into a two-body problem. We have engineered an expression construct in which a Hexa-Histidine tag is appended to the N-terminus of the single-chain IL-6/IL-6Rα complex through a thrombin-cleavable linker (Figure 1). This fusion construct was then produced in high yield as 75%-pure inclusion bodies in *Escherichia coli*, which were subsequently refolded into active material (the contaminant precipitated out of solution during refolding). Refolding of the single-chain complex ensures a stoichiometric ratio of IL-6 to IL-6-Rα, as well as reduces the entropic cost of individually expressed IL-6 and IL-6Rα complexing in dilute solution during refolding. A novel dilution refolding protocol was developed in which the concentration of protein is reduced simultaneously with dilution of denaturant using a controlled introduction of diluent. The Hexa-Histidine tag enables capture of the proteins from very dilute refolding solutions and results in a high proportion of correctly folded material. The eluant from the Ni-NTA agarose was then

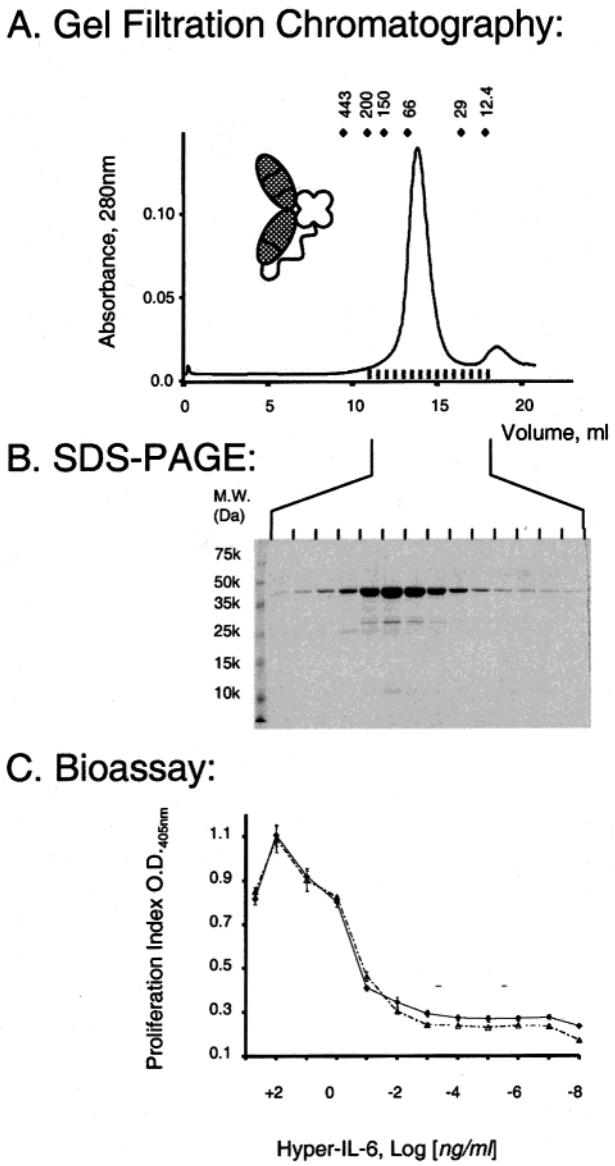

FIGURE 2: Biochemical analysis and biological activity of refolded hyper-IL-6. (A) Gel filtration chromatogram of refolded hyper-IL-6 showing a distinct peak eluting at ~45 kDa. The mobility markers are shown as diamond symbols and the unit is kDa. (B) Coomassie-stained SDS−PAGE analysis of the peak fractions shows the highly pure 45 kDa hyper-IL-6 band. (C) Bioassay of the purified hyper-IL-6 in supporting BAF/gp130 cell proliferation with potency better than 1 ng/mL (see Materials and Methods).

further purified via gel filtration chromatography (GFC). The harvested material behaves as a distinct single species eluting at approximately 45 kDa on the gel filtration chromatogram (Figure 2A). SDS−PAGE analysis (Figure 2B) demonstrates that there is a single protein migrating at ~45 kDa, corresponding to the expected theoretical Mr from the hyper-IL-6 amino acid sequence. Furthermore, the refolded hyper-IL-6 is biologically active, stimulating the growth of gp130-expressing BAF/gp130 cells which requires IL-6 and IL-6Rα for their growth (Figure 2C). The specific activity of the refolded material is at least as high as similar material produced from mammalian sources (*21*). Hyper-IL-6 was refolded in solution as an active monomer, exhibiting no tendency to dimerize or oligomerize by either gel filtration or analytical ultracentrifugation analysis. The yield of the active hyper-IL-6 is about 100−300 μg from 100 mg of inclusion bodies in a 1−2 L dilution volume. This yield of hyper-IL-6 is sufficient for extensive biochemical and biophysical studies of the molecule and its complex.

For gp130, we expressed domains 2 and 3, also termed the cytokine-binding homology region (CHR), as N-terminal-6xHis-tagged inclusion bodies in *E. coli*, which were then refolded. After refolding, and capture by Ni-NTA, the harvested material behaves as monomer on GFC (Figure 3A). SDS−PAGE analysis shows the refolded gp130 CHR is highly homogeneous. The refolded gp130 CHR tends to aggregate when warmed to 25 °C or higher. For this reason, most of the experiments involved with this protein were carried out at 20 °C or lower temperature. The yield is about 1 mg from 100 mg of inclusion bodies, significantly higher than that of hyper-IL-6. Equilibrium sedimentation analysis showed the gp130 CHR has a mass of 26.5 kDa vs the theoretical mass of 24.5 kDa.

With the ability to refold IL-6/IL-6Rα single-chain and gp130 individually, we then attempted complex formation by two methods: (1) mixing individually refolded hyper-IL-6 with the gp130 CHR, and (2) simultaneously refolding hyper-IL-6 with gp130 CHR ("cofolding"). Although both methods resulted in formation of the complex, the poor refolding yields of hyper-IL-6 limited the mixing strategy. Hence, cofolding resulted in substantially improved yields of hyper-IL-6 as judged by the large amount of hyper-IL-6/gp130 complex, and we could isolate by gel filtration. The refolded materials were captured using Ni-NTA agarose and purified with GFC as before (Figure 3C). The harvested material showed two distinct peaks, one which migrates at approximately 33 kDa (excess uncomplexed gp130 CHR), and the other at approximately 75 kDa. SDS−PAGE shows that the 75 kDa peak consists of two proteins, hyper-IL-6 and the gp130 CHR and is, therefore, a bimolecular complex. The elution position on the column suggests the complex is a 1:1 association of hyper-IL-6 and gp130 CHR. Quantitative N-terminal sequencing of the peak material indicates a 1:1 stoichiometry between the hyper-IL-6 and gp130 CHR (data not shown).

To more rigorously determine the molecular masses of both the free and liganded forms of the complexes in solution, we analyzed the proteins using sedimentation equilibrium analytical ultracentrifugation. The equilibrium sedimentation profiles of the individually refolded gp130 CHR, hyper-IL-6, co-folded and mixed hyper-IL-6 and gp130-CHR complexes can be fit with ideal curves and single molecular weight species distribution. According to these analyses, we calculate the Mr for gp130-CHR to be 26.5 kDa (theoretical, 24.5 kDa) and hyper-IL-6 is 45.4 kDa (theoretical, 46.8 kDa). The Mr for the mixed and cofolded complexes are 72.9 kDa and 68.6 kDa, respectively (theoretical, 71.3 kDa). Hence, the complex of hyper-IL-6 and gp130 CHR is a stable 1:1 heterodimer (or heterotrimer, i.e., IL-6-linker-IL-6Rα + gp130-CHR).

Interaction between the hyper-IL-6 and the gp130-CHR. We characterized both the mixed and cofolded trimolecular complexes by nondenaturing "native" gel electrophoresis at pH 8.0 to determine if there was quantitative complex formation or whether an excess of either component remained unbound when both molecules (hyper-IL-6 and gp130 CHR) were mixed or cofolded in stoichiometric ratios. Native gel can be a sensitive means of detecting complex formation

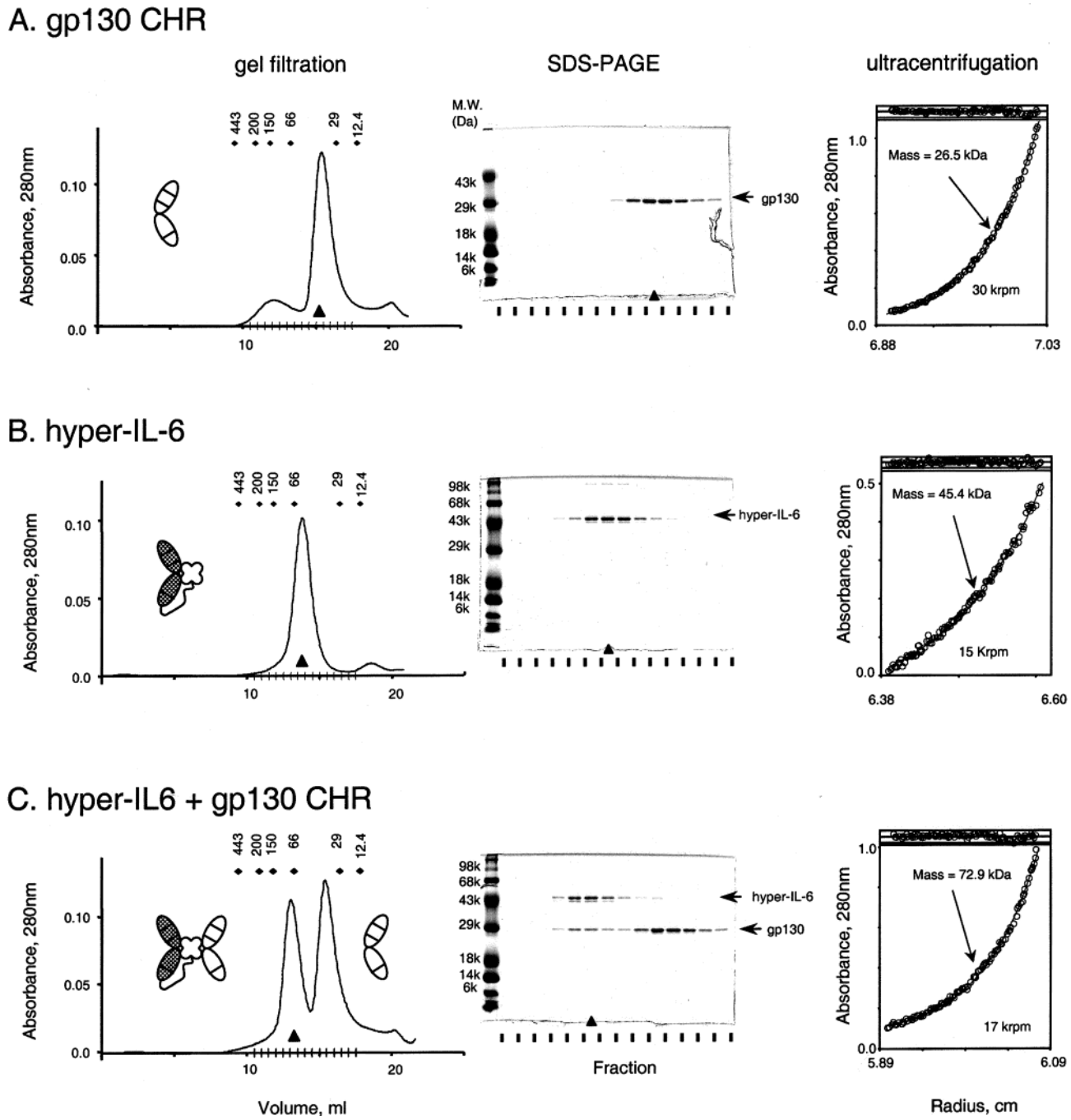

FIGURE 3: Biochemical analysis of the individual components and complex between hyper-IL-6 and gp130-CHR. (A) Refolded gp130-CHR. (B) Refolded hyper-IL-6. (C) Co-refolded hyper-IL-6 and gp130-CHR. At the left of each panel is the gel filtration chromatography profile (superdex-200), in the middle is the coommassie-stained SDS−PAGE gel of the peak fractions bracketed by the hash marks, and at the right is the sedimentation equilibrium profile of the peak fraction indicated by the triangle. For the co-folded hyper-IL-6/gp130-CHR, an excess of the gp130 is present due to its substantially higher refolding efficiency. All the proteins behave very close to their theoretical Mr (gp130-CHR, 24.5 kDa; hyper-IL-6, 46.8 kDa; hyper-IL-6/gp130-CHR, 71.3 kDa).

between interacting proteins, which is often indicated by band-shifting (*25*). We used native gel to analyze the hyper-IL-6, gp130 CHR and their complex (Figure 4). The multiple bands of the refolded hyper-IL-6 indicates that the protein has some conformational heterogeneity, which is observed on native gels of many recombinant proteins, and may reflect the flexibility of the linker peptide (Figure 4, lane 1). The refolded gp130 CHR has a mobility distinct from hyper-IL-6, and migrates as a sharper band (Figure 4, lane 2). In the sample mixture of individually refolded hyper-IL-6 and gp130 CHR, a complex formed as evidenced by a protein band distinct from the either protein alone (Figure 4, lane 3). Interestingly, this mixed complex has different mobility than the cofolded complex (Figure 4, lane 4). This suggested the two hetero-dimers might be in different conformational states, since both complexes have the same retention time on GFC (data not shown).

To measure the affinity of hyper-IL-6 and gp130 CHR, we analyzed the interaction between hyper-IL-6 and gp130 CHR by surface plasmon resonance (SPR) using both kinetic and equilibrium analysis. After immobilizing gp130 CHR, we flowed various concentrations of hyper-IL-6 over it and

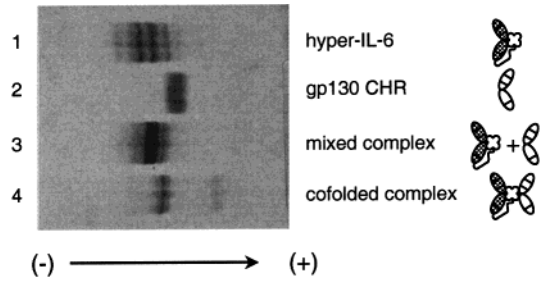

FIGURE 4: Native gel analysis of the components of the complexes. Native gel analysis of refolded hyper-IL-6 (lane 1), refolded gp130 CHR (lane 2), equimolar mixed (1:1) individually refolded hyper-IL-6 and gp130 CHR (lane 3), and co-folded complex purified by gel filtration chromatography (lane 4).

the SPR signal of interaction was monitored on a BIAcore 1000 machine. Figure 5A shows a typical set of sensorgrams of various concentrations of hyper-IL-6 on a 600 RU gp130 CHR surface, corrected for blank surface binding. We encountered a technical problem that high concentrations of injected analyte (hyper-IL-6) required extended wash times to completely return to baseline. Therefore, we approximated the dissociation constant (K_D) using scatchard plot analysis. Since the maximum levels of the sensorgrams are almost, but not absolutely, flat, we selected a value (very close to the maximum value) for each sensorgram and treated the values as the equilibrium levels, then carried out a scatchard plot analysis (Figure 5B). We sought to minimize injection times in order to prevent rebinding artifacts, and we also carried out the measurements at a range of gp130 coupling densities. Binding studies were performed at 20 °C and lower (data not shown) to minimize a tendency of gp130 to aggregate at temperatures above 20 °C. However, the final K_D determined from the scatchard should be considered approximate due to the complications introduced by the baseline shift at high concentrations. With these caveats in mind, we can approximate a K_D from the scathcard plot of 52 nM. The hyper-IL-6 loses activity upon coupling to the BIAcore chip so the experiments cannot be carried out in the reverse orientation. Isothermal titration calorimetry experiments with the identical material confirms this K_D (data not shown).

To estimate K_D from on and off-rate, we were unable to fit the data to a 1:1 langmuir model, but can be fit best with a two-state interaction model (Figure 5, panels C and D). These yielded a K_D of 31 nM. The K_Ds are different from these two methods, but within 50% of each other, and may, in part, provide a basis for rationalizing the different mobility between mixed and cofolded complexes as seen in native gel. However, whether the two-state model is a bona fide property of the IL-6/gp130 recognition or simply a function of the surface chip immobilization of the gp130, remains to be determined through structural analysis. The relative similarity of the equilibrium and kinetic values indicate that our approximation of this K_D is reasonably accurate, although not highly precise, due to the problematic gp130 behavior, but is satisfactory given the limitations we encountered.

A longstanding question about IL-6 is the composition of the higher-order signaling complex (*26*). The complex of IL-6/IL-6Rα and the CHR of gp130 constitutes the minimal "recognition" complex but an additional N-terminal Ig-like (IGD) domain of gp130, also termed D1, is required for

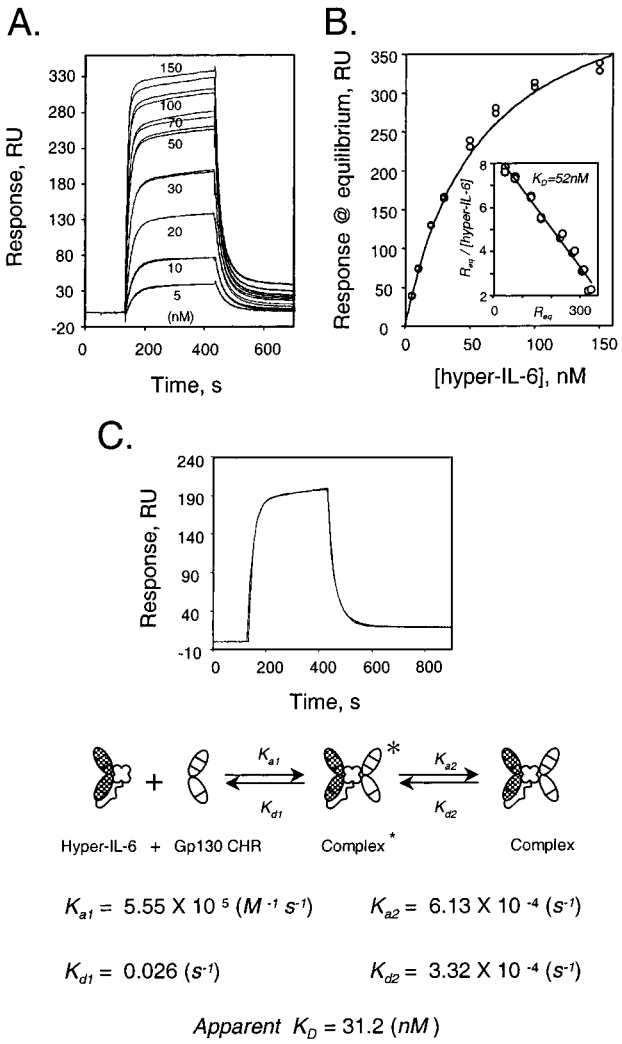

FIGURE 5: Surface plasmon resonance analysis of the interaction between hyper-IL-6 and gp130-CHR. (A) SPR experiment showing sensorgrams of injections of different concentrations of hyper-IL-6 over a chip with 600RU of immobilized gp130-CHR (sensorgrams are background-subtracted). Each concentration was done in duplicate, and the measurements have been reproduced over a range of gp130 coupling densities. To minimize background and correct for any nonspecific effects, 100 μg/mL BSA is included in the hyper-IL-6 injection buffer. The baseline shift at high hyper-IL-6 concentrations returns to baseline after longer wash times. Subtractions were made for blank surface. (B) Scatchard plot analysis of sensorgrams. The final K_D determined from the scatchard should be considered approximate due to the complications introduced by the baseline shift at high concentrations. (C) Kinetic determination of K_D by fitting of a representative sensorgram with a two-state model. Response sensorgrams in panel A were fitted with this model and yield the parameters shown here. Using this model, there is a "meta state" of the hyper-IL-6/gp130-CHR complex which precedes the final state.

signaling, and we refer to this complex as the "activation" complex (*12*). We attempted to reconstitute the activation complex to compare it to the recognition complex.

We were unable to express the functional three-domain gp130 IGD-CHR fragment in *E. coli*. Hence, we expressed the gp130 IGD-CHR module, as well as hyper-IL-6, in insect cells using the baculovirus system. The hyper-IL-6 from insect cells and *E. coli* behave identically on gel filtration and bioactivity assays, providing further evidence that our refolded hyper-IL-6 is in the correct conformation. When the insect cells were co-infected with both gp130 IGD-CHR

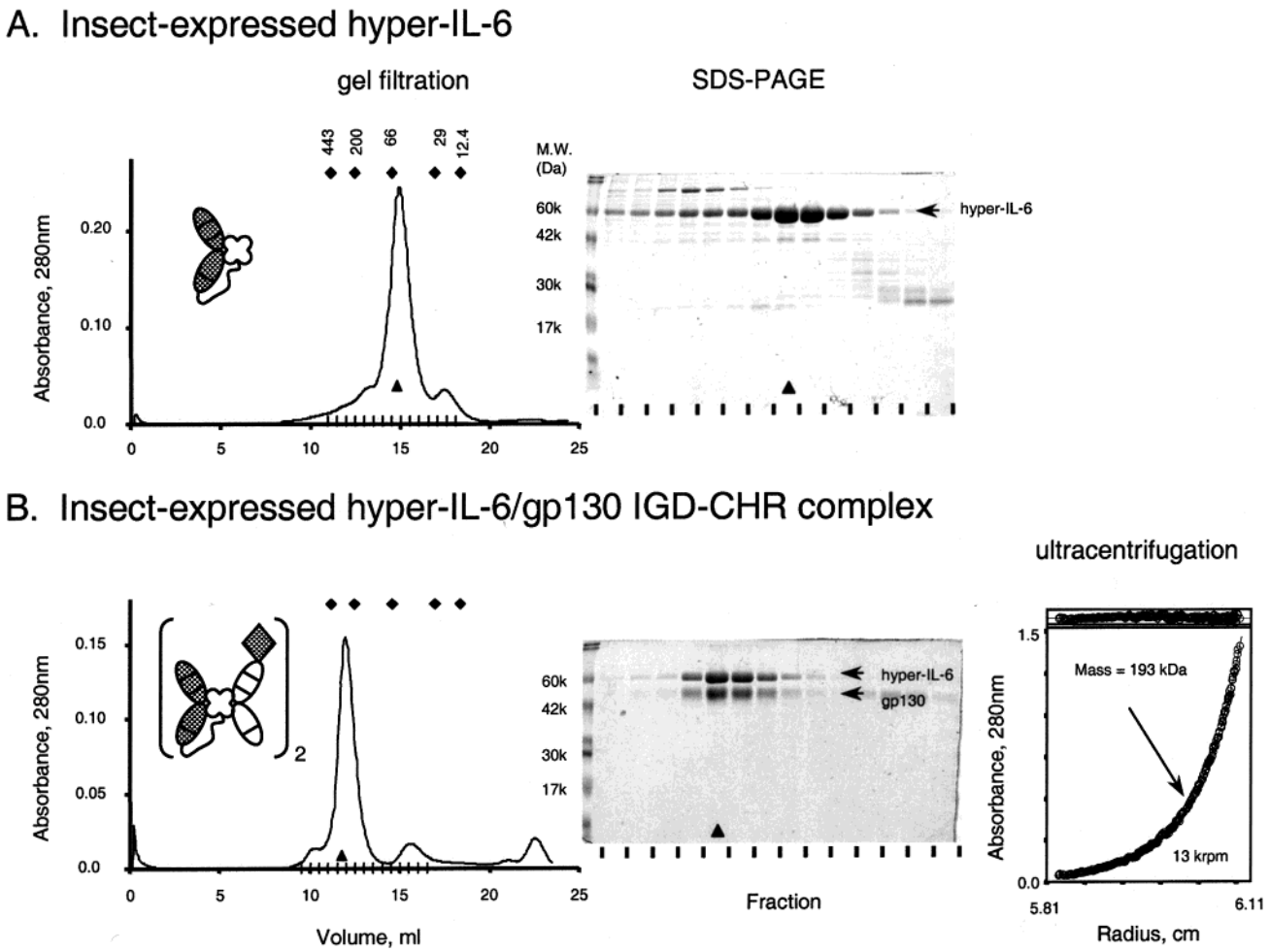

FIGURE 6: Hyper-IL-6 forms a hexamer with gp130-IGD-CHR expressed from insect cells. (A) Hyper-IL-6 and (B) its complex with the D1D2D3 domains of gp130 (IGD-CHR) were expressed using the baculovirus system. The secreted complexes were harvested from the culture supernatant via Nickel-agarose, and further purifed by gel filtration chromatography, as shown in the left panel. The insect-expressed hyper-IL-6 behaves identically to the refolded material, but elutes at a slightly higher MW due to glycosylation from the insect cells not present in the *E. coli* material. At the right, sedimentation equilibrium analysis of hyper-IL-6 (A) and the hyper-IL-6/gp130-IGD-CHR hexameric complex reveal masses (Mr) which correlate well with expected theoretical values. The broad banding patterns seen in the coommassie-stained SDS−PAGE are indicative of glycosylation heterogeneity (six N-linked sites on gp130, four on hyper-IL-6). Note that the hyper-IL-6/gp130-IGD-CHR hexameric complex elutes at ~220 kDa on gel filtration, which is larger than seen by ultracentifugation. This is due to the extended structure of the hexameric assembly compared to the relatively symmetric globular structure of the heterotrimer.

and hyper-IL-6 viruses, large quantities of complex were readily harvested by Ni-NTA resin and further purified in either gel filtration or anion exchange chromatography (Figure 5). Gel filtration chromatography of the complex shows that the complex has a MW of ~200 000. We can also form this complex by mixing individually purified hyper-IL-6 and gp130-IGD-CHR (data not shown). Because of heavy glycosylation, both hyper-IL-6 and gp130 IGD-CHR run as broad bands with higher Mr than their core polypeptide Mr. (four N-linked glycosylation sites on hyper-IL-6, six N-linked glycosylation sites on gp130). This purified complex was then analyzed by both equilibrium sedimentation and velocity ultracentrifugation which showed that the hyper-IL-6/gp130 IGD-CHR behaved as a monodisperse species with a mass of 193 kDa (theoretical mass 191.6 kDa, which indicates a 2:2:2 hexameric stoichiometry.

We attempted to measure the affinity of hyper-IL-6 for gp130-IGD-CHR using surface plasmon resonance; however, the gp130-IGD-CHR does not couple satisfactorily to the BIAcore chip surface, and so we do not report these measurements. However, it is known from previous studies that the affinity of IL-6/IL-6Rα for full-length gp130 is ~0.1 nM (*12*), and this high affinity is consistent with the extreme stability of our hyper-IL-6/gp130-IGD-CHR in solution even at dilute concentrations. Hence, we believe the gp130 D1D2D3 fragment contains all binding epitopes necessary to account for the entire high-affinity signaling complex. Preliminary calorimetry experiments between hyper-IL-6 and gp130-IGD-CHR confirm the substantially higher-affinity of this complex compared to the hyper-IL-6/gp130-CHR affinity.

Hydrodynamic Properties of the Complexes. To further characterize the hydrodynamic properties of the complexes, velocity sedimentation analysis was carried out. The result of d*c*/d*t* analysis (Figure 7, curve 1) shows that the hyper-IL-6/gp130 CHR complex behaves as a homogeneous single species with a sedimentation coefficient of 3.5 S and the *D* is (~13F). Using the sedimentation coefficient of 3.5 S and the 75 kDa as the mass, we estimated the f/f_{min} to be 1.79. The derived Stokes radius is 50 Å, while the sphere model has a radius of 28 Å. For hyper-IL-6/gp130 IGD-CHR (hexameric) complex the sedimentation velocity analysis

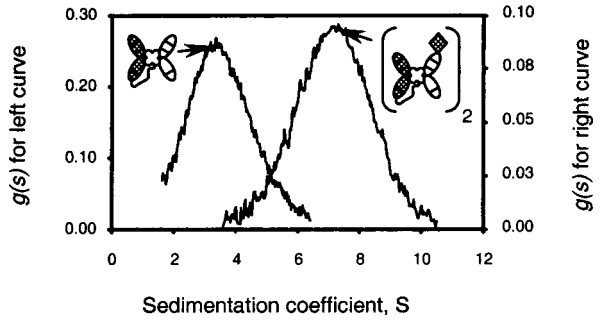

FIGURE 7: Sedimentation velocity analysis of the heterotrimeric hyper-IL-6/gp130-CHR complex and the hexameric hyper-IL-6/gp130-IGD-CHR complex. The results of d*c*/d*t* analysis indicates that both complexes behave monodispersely in solution with a *s* value around 3.5S for hyper-IL-6/gp130 CHR complex and an *s* value around 7.16S for hyper-IL-6/gp130 IGD-CHR complex. The velocity sedimentation of hyper-IL-6/gp130 CHR complex was carried out at 45 000 rpm at 15 °C and hyper-IL-6/gp130 IGD-CHR at 35 000 rpm at 20 °C. All the calculations were corrected to 20 °C standard.

estimated $s = 7.16$S and $D = \sim$4F. On the basis of 7.16S and 195 kDa mass, we estimated f/f_{min} of 1.65 with derived Stoke radius of 63.5 Å and sphere model radius of 38.5 Å. Note that the *D* value gives a Stoke radius 52.6 Å, suggesting the preparation is highly homogeneous.

DISCUSSION

Our purpose in this study was to utilize a novel tethering strategy to produce a single-chain cytokine/receptor complex for biochemical and biophysical studies addressing the interaction of IL-6, a representative gp130-cytokine, with gp130. This type of analysis has long been complicated by the fact that IL-6, as well as other gp130-cytokines, must first complex with a specific α-receptor, to bind to gp130. Hence, it has been difficult to deconvolute the discrete interaction of the IL-6/IL-6Rα complex with gp130 in the face of a three-component system. In our single-chain, or "hyper", cytokine, dissociation of IL-6 and its Rα is eliminated, and so the three-component complex of IL-6/IL-6Rα and gp130 is effectively reduced to a bimolecular interaction. In this fashion, we can discretely measure complex formation between the composite interface of IL-6/IL-6Rα and the gp130. Using this strategy, we have directly addressed questions about the assembly of the IL-6/IL-6Rα/gp130 signaling complex which are important for understanding the biology of this system.

The tethering strategy was successful in producing a refolded single-chain cytokine receptor complex, which is the first example we know of a "one-pot" refolding of a cytokine/receptor complex. This strategy, then, which was initially developed with the intent of producing hyperactive cytokines for therapeutic purposes, is also a convenient method for producing bimolecular complexes for biophysical studies. The biological potency of the hyper-IL-6 is 10−100-fold greater than the unlinked IL-6 and IL-6Rα (*21*). The linking of IL-6 and IL-6Rα ensures that all the molecules are the biologically active IL-6/Rα complex, whereas the normal physiological concentration of free IL-6 is on the order of 10^{-9} M, which results in a substantial fraction of uncomplexed, inactive cytokine. This is very similar to the situation of IL-12 (*27*), which is composed of two disulfide-linked subunits similar to the IL-6/IL-6Rα complex. A single-chain strategy has been successfully utilized for expression of other covalently linked heterodimers such as single-chain Fv fragments of antibodies (*28*), but hyper-IL-6 is the first application of a covalent linkage strategy between receptor and ligand to enhance the cytokine potency. The technique is applicable to numerous other cytokine receptor systems, and has recently been demonstrated with a single-chain IL-11/IL-11Rα complex (*29*).

The single-chain IL-6/IL-6Rα complex is monomeric even at high concentrations, as judged by both gel filtration chromatography and analytical ultracentrifugation. Hence, it is likely that the IL-6/IL-6Rα complex is also monomeric on the cell surface, although our solution measurements cannot rule out the possibility of preassembled oligomers of the IL-6/IL-6Rα complex on the cell surface, as has been shown for other hematopoietic receptors such as EPO-R (*30*, *31*). The refolded single-chain complex was very active in stimulating proliferation of BAF/gp130 cells expressing gp130, through the process of transignaling, which is a known phenomenon exhibited by "shed" IL-6/IL-6Rα complexes in diseases such as multiple myeloma. Both our refolded, and insect-expressed single-chain complexes are at least 10−100-fold more active at stimulating BAF/gp130 cells than individually produced soluble IL-6 and IL-6Rα, verifying the design concept that tethering the cytokine and receptor together eliminates dissociation, resulting in a more potent molecule. This also confirms that the absence of posttranslational modifications in the *E. coli* produced material has no effect on biological activity.

The single-chain IL-6/IL-6Rα complex was then analyzed for interaction with the CHR of gp130. Prior to this study, the characteristics of the interaction of LC (long-chain) cytokine/Rα complexes with the CHR of gp130 (or related signal transducers such as LIF-R) were not well understood. The reasons for this are that (1) neither cytokine nor Rα bind the gp130 CHR alone, but require preformed complex, which introduces experimental difficulties, and (2) the N-terminal IGD-, or D1 domain, of gp130 is necessary for signaling, presumably through interaction of the unique site III on IL-6. Thus, a goal of our study was to separate the "recognition" complex composed of IL-6/ IL-6Rα/gp130-CHR from the "activation" complex that includes the D1 domain of gp130. Does the gp130 CHR bind to the IL-6/IL-6Rα complex in the absence of D1 and, if so, what is the affinity and stoichiometry of this interaction?

For this purpose, we refolded the CHR of gp130 in high yield, and determined by both GFC and sedimentation analysis that the CHR is monomeric. We used GFC, native gel electrophoresis, surface plasmon resonance, and analytical ultracentrifugation to measure the interaction of the refolded single-chain IL-6/IL-6Rα with the refolded gp130 CHR. By GFC and AU, hyper-IL-6 and the CHR form a stable complex either by mixing independently refolded proteins or simultaneously refolding. By GFC, the complex peak is clearly distinct from the uncomplexed peak and chromatographs at a Mr of ~70 kDa. This Mr is indicative of a 1:1:1 complex of one IL-6, one IL-6Rα, and one gp130 CHR. Using analytical ultracentrifugation, the GFC results are recapitulated, showing in addition excellent fits to a monodisperse model of the bi- and trimolecular complexes. This "monomeric" trimolecular complex then defines the minimal

"recognition" complex and demonstrates that the CHR alone of gp130 is capable of forming relatively high affinity interactions with the IL-6/IL-6Rα complex in the absence of the D1 domain. This hetero-trimeric complex, then, resembles the homo-dimeric complexes such as GH and EPOR, and allows us to postulate that the IL-6/IL-6Rα/gp130-CHR heterotrimer assembly resembles the hGH/GH-receptor complex.

Interestingly, analysis of the hyper-IL-6/gp130 complex by nondenaturing native gel electrophoresis reveals differences in both the position and banding pattern of the complexes. First, both mixed and cofolded complexes clearly form stable complexes using this method, as the positions of the complex differ significantly from the individual hyper-IL-6 and gp130. The cofolded complex is essentially a single band, whereas the mixed complex is a collection of bands, none of which appear to be dissociated components. What is the basis for this difference? We know from our other results that the differences are not due to an alternative stoichiometry or molecular size of the mixed versus cofolded complexes. Native gel can be extremely sensitive to subtle conformational differences in proteins. For example, native gel is a reliable indicator of peptide-loading of MHC molecules through obvious band shifts (*32*). Conformational heterogeneity is usually indicated by multiple native gel bands, whereas more rigid structures are sharper and more homogeneous. Hence, in our case, it is possible that, during the process of co-folding, the binding sites of hyper-IL-6 and gp130 have achieved a more complementary fit through simultaneously sampling conformational space and adapting to each other's binding site. Conversely, the individually refolded and then mixed proteins may have folded into their stable structures, which represent energy minima, which are then limited in their ability to adapt to each other's binding surface. These are speculations, but it is a fact that the D1 domain of gp130 is required for signaling through interaction with site III of IL-6 and formation of a higher-order structure. It is likely, then, that an initial trimolecular complex forms through the minimal recognition complex we have shown here, and then the D1-site III interaction drives a conformational transition into the higher-order, more stable signaling complex.

Surface plasmon resonance analysis of the affinity of the gp130 CHR interaction reveals an approximate affinity between 30 and 50 nM. Despite the less-than-optimal behavior of the gp130 CHR on the BIAcore chip (as evidenced through baseline drift at high analyte concentrations), it is very clear that this affinity is 1−2 orders of magnitude weaker than cytokine interactions with the CHR of their receptors measured to date, affinities which are normally in the sub-nanomolar range. The lower affinity is not due to incorrectly folded hyper-IL-6 since both material secreted from insect cells and the refolded protein exhibit the same affinity and bioactivity. The explanation for this is likely that the CHR of gp130 is *not* the complete signaling complex, but is the "minimal" recognition complex. A conformational transitions occurs following engagement of the gp130 CHR to a higher-order complex, and so the affinity of the initial recognition complex cannot be so high that further remodeling of the complex cannot occur, a similar situation was reported between OSM and gp130 (*10*). For other cytokines such as hGH and EPO, homodimerization of their receptor CHRs is sufficient to activate the receptors, so the initial affinity of the cytokine for the CHR is correspondingly higher. The affinity between the gp130 CHR and the hyper-IL-6 is about 2 orders-of-magnitude less than the reported affinity of IL-6 and full-length gp130 (0.1 nM) (*33*). This suggests the importance of other domains, especially IGD, of gp130 in enhancing the affinity through interaction with site III of IL-6. Hence, the sequential mode of receptor interaction rationalizes the hierarchical increase in binding affinity from the initial binding event of the IL-6/IL-6Rα complex to the gp130 CHR, followed by engagement of site III by D1.

The kinetic measurements are best fit to a two-state model in which an intermediate "meta" state undergoes a conformational transition into a stable final state. We recognize the possible technical artifacts of BIAcore measurements from the surface immobilization, and so we do not overinterpret this result. However, this observation is supported by preliminary studies we have carried out indicating a temperature-dependent binding kinetics between hyper-IL-6 and gp130, which is indicative of conformational adjustment in the binding surface (data not shown). The existence of the two-state model, as observed in the kinetic experiments, could significantly affect the apparent affinity depending upon the cytokine and receptor interaction duration (since the reported value of full-length gp130 was measured with the incubation time of hours while our BIAcore measurement only lasted minutes). The two-state characteristic of the interaction between the hyper-IL-6 and the gp130 CHR may significantly increase the apparent affinity over long incubation times with sustained levels of hyper-IL-6 (Figure 1C). Hence, the two-state model may reflect the transition that must take place during the stepwise reorganization from the trimolecular recognition complex to the hexameric signaling complex. An alternative explanation consistent with the data would involve conformational heterogeneity of the ligand or receptor, with slow and fast binding forms. The two-state nature of the interaction remains a phenomenon requiring further study.

Finally, we produced a version of gp130 including all three N-terminal domains, constituting the IGD (D1) plus the CHR (D2D3). We were unable to express this larger fragment in *E. coli*, and so resorted to insect cells, which secreted the active molecule. Coexpression of this three-domain fragment with hyper-IL-6 resulted in a hexameric complex when measured by gel filtration and analytical ultracentrifugation. Hence, the IGD is necessary for recruitment into the higher order-signaling complex. The hexameric stoichiometry has been previously observed in both the IL-6, IL-11, and CNTF systems (*18*−*20*). However, our ability to reconstitute this hexamer in large quantitities for rigorous biophysical analysis extends, and recapitulates, the functional data. We can then postulate an assembly mechanism in which the IL-6/IL-6Rα complex first engages the gp130 CHR, followed by recruitment of the IGD by the IL-6 site III into the active assembly. We cannot rule out that the site II of IL-6 may interact with the gp130 CHR simultaneous to site III interaction with the IGD, but the fact that (1) IL-6/IL-6Rα complexation is a prerequisite for any interaction between IL-6 and gp130, and (2) IL-6/IL-6Rα/gp130-CHR forms a stable complex in the absence of the D1 strongly infers that the order of assembly starts with site II followed by oligomerization into/via site

III. Attempts to measure a discrete affinity between the cytokine and site III are in progress.

In conclusion, we have utilized a tethering strategy to overcome the technical difficulties which have, until now, prevented the in vitro reconstitution of the recognition and activation complexes between IL-6/IL-6Rα and gp130. This tethering strategy has allowed us to clearly determine the stoichiometry of this complex with soluble molecules and measure the binding constants of the bimolecular complex interaction with the gp130 CHR. Although the composition of the trimolecular "recognition" complex is clearly 1:1:1, we observe an interesting heterogeneity between complexes formed by mixing or cofolding, and this heterogeneity may be reflected in the kinetic rate constants measured by surface plasmon resonance. In the future, structural studies will focus on both the mixed and cofolded complexes to determine which, if any, structural differences exist. We have also reconstituted the hexameric activation complex, clearly demonstrating the importance of the IGD in cross-linking the two recognition complexes into a hexameric activation complex.

ACKNOWLEDGMENT

The authors gratefully acknowledge the contributions of Fernando Bazan, Rob Kastelein, Birgitt Oppman, Andy Snow, John Xiu, and Michelle Krogsgaard. We also acknowledge the Theriot lab for use of the ultracentrifuge and the Davis lab for use of the BIAcore. DCC is supported by a postdoctoral training grant to the Department of Microbiology & Immunology, and K.C.G. is supported by the Cancer Research Institute, the California Cancer Research Program, a Rita Allen Foundation award, a Frederick Terman Junior Faculty award, NIH (RO1-AI-48540-01), and startup funds provided by The Stanford University School of Medicine.

REFERENCES

1. Ihle, J. N., Witthuhn, B. A., Quelle, F. W., Yamamoto, K., and Silvennoinen, O. (1995) *Annu. Rev. Immunol. 13*, 369−98.
2. Hibi, M., Nakajima, K., and Hirano, T. (1996) *J. Mol. Med. 74*, 1−12.
3. Kishimoto, T., Akira, S., Narazaki, M., and Taga, T. (1995) *Blood 86*, 1243−54.
4. Taga, T., and Kishimoto, T. (1997) *Annu. Rev. Immunol. 15*, 797−819.
5. Bravo, J., and Heath, J. K. (2000) *EMBO J. 19*, 2399−411.
6. Hibi, M., Murakami, M., Saito, M., Hirano, T., Taga, T., and Kishimoto, T. (1990) *Cell 63*, 1149−57.
7. Simpson, R. J., Hammacher, A., Smith, D. K., Matthews, J. M., and Ward, L. D. (1997) *Protein Sci. 6*, 929−55.
8. Bazan, J. F. (1990) *Proc. Natl. Acad. Sci. U.S.A. 87*, 6934−8.
9. Grotzinger, J., Kurapkat, G., Wollmer, A., Kalai, M., and Rose-John, S. (1997) *Proteins 27*, 96−109.
10. Staunton, D., Hudson, K. R., and Heath, J. K. (1998) *Protein Eng. 11*, 1093−102.
11. Moritz, R. L., Hall, N. E., Connolly, L. M., and Simpson, R. J. (2000) *J. Biol. Chem*.
12. Hammacher, A., Richardson, R. T., Layton, J. E., Smith, D. K., Angus, L. J., Hilton, D. J., Nicola, N. A., Wijdenes, J., and Simpson, R. J. (1998) *J. Biol. Chem. 273*, 22701−7.
13. Wells, J. A., Cunningham, B. C., Fuh, G., Lowman, H. B., Bass, S. H., Mulkerrin, M. G., Ultsch, M., and deVos, A. M. (1993) *Recent Prog. Horm. Res. 48*, 253−75.
14. Wilson, I. A., and Jolliffe, L. K. (1999) *Curr. Opin. Struct. Biol. 9*, 696−704.
15. Inoue, M., Nakayama, C., Kikuchi, K., Kimura, T., Ishige, Y., Ito, A., Kanaoka, M., and Noguchi, H. (1995) *Proc. Natl. Acad. Sci. U.S.A. 92*, 8579−83.
16. Kurth, I., Horsten, U., Pflanz, S., Timmermann, A., Kuster, A., Dahmen, H., Tacken, I., Heinrich, P. C., and Muller-Newen, G. (2000) *J. Immunol. 164*, 273−82.
17. Kallen, K. J., Grotzinger, J., Lelievre, E., Vollmer, P., Aasland, D., Renne, C., Mullberg, J., Myer zum Buschenfelde, K. H., Gascan, H., and Rose-John, S. (1999) *J. Biol. Chem. 274*, 11859−67.
18. Paonessa, G., Graziani, R., De Serio, A., Savino, R., Ciapponi, L., Lahm, A., Salvati, A., Toniatti, C., and Ciliberto, G. (1995) *EMBO J. 14*, 1942−1951.
19. Ward, L., Howlett, G., Discolo, G., Yasukawa, K., Hammacher, A., Moritz, R., and Simpson, R. (1994) *J. Biol. Chem. 269*, 23286−23289.
20. Barton, V. A., Hall, M. A., Hudson, K. R., and Heath, J. K. (2000) *J. Biol. Chem. 275*, 36197−36203.
21. Fischer, M., Goldschmitt, J., Peschel, C., Brakenhoff, J. P., Kallen, K. J., Wollmer, A., Grotzinger, J., and Rose-John, S. (1997) *Nat. Biotechnol. 15*, 142−5.
22. Laue, T. M., Shah, B. D., Ridgeway, T. M., Pelletier, S. L. in *Analytical Ultracentrifugation in Biochemistry and Polymer Science* (Harding, S. E., Rowe, A. J., Horton, J. C., Eds.) pp 90−125, Royal Society of Chemistry, Cambridge, U.K.
23. Stafford, W. F. d. (1992) *Anal. Biochem. 203*, 295−301.
24. Oppmann, B., Stoyan, T., Fischer, M., Voltz, N., Marz, P., and Rose-John, S. (1996) *J Immunol. Methods 195*, 153−9.
25. Degano, M., Garcia, K. C., Apostolopoulos, V., Rudolph, M. G., Teyton, L., and Wilson, I. A. (2000) *Immunity 12*, 251−61.
26. Grotzinger, J., Kernebeck, T., Kallen, K. J., and Rose-John, S. (1999) *Biol. Chem. 380*, 803−13.
27. Yoon, C., Johnston, S. C., Tang, J., Stahl, M., Tobin, J. F., and Somers, W. S. (2000) *EMBO J. 19*, 3530−41.
28. Fields, B. A., Goldbaum, F. A., Dall'Acqua, W., Malchiodi, E. L., Cauerhff, A., Schwarz, F. P., Ysern, X., Poljak, R. J., and Mariuzza, R. A. (1996) *Biochemistry 35*, 15494−503.
29. Pflanz, S., Tacken, I., Grotzinger, J., Jacques, Y., Minvielle, S., Dahmen, H., Heinrich, P. C., and Muller-Newen, G. (1999) *FEBS Lett. 450*, 117−22.
30. Livnah, O., Stura, E. A., Middleton, S. A., Johnson, D. L., Jolliffe, L. K., and Wilson, I. A. (1999) *Science 283*, 987−90.
31. Remy, I., Wilson, I. A., and Michnick, S. W. (1999) *Science 283*, 990−993.
32. Stratmann, T., Apostolopoulos, V., Mallet-Designe, V., Corper, A. L., Scott, C. A., Wilson, I. A., Kang, A. S., and Teyton, L. (2000) *J. Immunol. 165*, 3214−25.
33. Moritz, R. L., Ward, L. D., Tu, G. F., Fabri, L. J., Ji, H., Yasukawa, K., and Simpson, R. J. (1999) *Growth Factors 16*, 265−78.

BI010192Q